Development and optimisation of a Near-Infrared spectroscopic system for glucose quantification in aqueous and intralipid-based samples

Nicholas B Davison[a*], Christopher J Gaffney[a], Jemma G Kerns[a], Qiandong Zhuang[b]

[a]*Lancaster Medical School, Lancaster University,, Lancaster, LA1 4AT, United Kingdom*
[b]*Physics Department, Lancaster University, Lancaster, LA1 4YW, United Kingdom*
*n.davison@lancaster.ac.uk

Abstract

A non-invasive glucose sensing device could revolutionise diabetes treatment. Near Infrared (NIR) spectroscopy is a promising technology for glucose sensing; however, the design and choice of components for NIR spectroscopy can greatly affect the sensing accuracy. We aimed to develop a NIR absorption spectroscopy system to determine liquid glucose concentrations in the physiological range, by evaluating a range of NIR photodetector components and light sources. Three detection assemblies were tested: (i) a dispersive spectrometer with photodiode array, (ii) a Czerny-Turner monochromator with InGaAs photodiode and (iii) a miniature Fourier Transform Infrared (FTIR) spectrometer. A halogen lamp and NIR globar were trialled as potential light sources. The components were systematically tested by comparing the coefficient of determination and standard error of prediction (SEP) for the same set of aqueous glucose samples through 10 mmol/L concentration steps. The Czerny-Turner monochromator with InGaAs photodiode, along with the globar, were identified as the optimal components for the system. A range of concentration steps (1-10 mmol/L) were scanned to identify the physiologically relevant limit of detection, which was identified as 5mmol/L for glucose in solution. Spectra were then collected from glucose samples in 10% intralipid suspension in the 10-20 mmol/L range and the equivalent concentrations in solution. The SEP was greater for the intralipid samples due to strong scattering. Scattering was dominant above 1300nm, whilst absorption was dominant below 1300nm. Although alternative approaches achieve better resolution, our system uses simple and readily-available components and presents a platform for a non-invasive NIR glucose sensing device.

Keywords: Near Infrared Spectroscopy, Glucose monitoring, Non-invasive sensing, Optical system design

1. Introduction

Controlling and monitoring glucose concentration is essential in the management of diabetes and research continues into developing a truly non-invasive glucose monitoring device [1]. Insulin is produced by β-cells of the pancreas and promotes glucose uptake into skeletal muscle, where glucose is broken down and used to generate and maintain glycaemic control. Diabetes mellitus is a metabolic condition and is classified into two categories, type 1 and type 2; type 1 in which insulin

is not produced by the β-cells and type 2 in which the skeletal muscle and other tissues become resistant to insulin [2]. The condition leads to complications associated with elevated glucose levels (hyperglycaemia), including diabetic retinopathy, nephropathy, neuropathy and increased risk of heart attack and stroke [3]. Diabetes presents a huge challenge to healthcare systems worldwide [4] especially as prevalence of the disease is rising, having risen from 108 million to 536 million between 1980 [5] and 2021 [6] and expected to increase further. To enable large numbers of people with diabetes to regularly track their blood glucose levels, an easy method of blood glucose monitoring is highly desirable.

People with diabetes typically measure their blood glucose concentration several times per day using a glucose meter, which involves pricking the finger with a needle to draw a small volume of blood onto a test strip, which is then analysed via a glucose-oxidase reaction in the test meter [7]. The main disadvantage of such meters is that they are invasive and inconvenient for patients and cannot offer continuous monitoring. Continuous subcutaneous glucose monitors, implanted under the skin, are an alternative method which allow glucose concentrations to be monitored continuously and tracked digitally [8,9]. However, they must be regularly replaced, at a significant cost to the health service, or user, and are still invasive. Hence, research continues to develop a truly non-invasive device.

Most approaches to non-invasive glucose sensing have been either optical, based on light and its various interactions with glucose in tissue, or non-optical approaches such as transdermal and electrochemical methods [10]. The first commercially available non-invasive glucose monitor, the GlucoWatch, used reverse iontophoresis, a transdermal technique that uses electrolysis to generate a concentration gradient with which to collect glucose molecules from the skin [11]. It was discontinued to due irritation issues and failing to detect rapid changes. Other transdermal methods have been investigated, notably bioimpedance, which uses small electric currents across a range of frequencies to measure resistance and reactance of the interstitial fluid [12,13]. Several studies in human subjects using bioimpedance have been reported, although the precise mechanism between bioimpedance and blood glucose is still not fully understood [14]. Research into electrochemical sensors that analyse glucose in sweat and tears [15] has also been reported, though the low glucose concentration and need for regular calibrations are challenges which must be overcome.

A range of optical technologies offer potential for glucose monitoring. These include Optical Coherence Tomography (OCT), which is an interferometry-based method where the gradient of the OCT signal slope can be correlated to the reduced scattering coefficient [16] and thus to glucose concentration. One major challenge is that other analytes also affect the scattering coefficient, though the effects may be weaker than that from glucose [17,18] and the technique has been tested in human subjects [19,20] with promising results. Raman spectroscopy is another optical method, which has also been tested in humans [21,22]. This technique has a major advantage that water has a very weak Raman signal, however Raman spectra can be affected by scattering from the skin and the signal intensity is often weak. Polarimetry [23] and photoacoustic spectroscopy (PAS) [24,25] based studies have also been reported.

Infrared spectroscopy measures the absorption of infrared radiation by glucose and other analytes, since every analyte will have a unique absorption spectrum which corresponds to vibrational modes within the molecule. Absorption in media is characterised by the Beer-Lambert Law [26,27], which describes the exponential relationship between light intensity at a given distance and concentration. However, the law alone does not suffice when considering light transport in tissue owing to the presence of scattering, reflection effects and the optical inhomogeneity of tissue. In practice, reflected light is usually collected and analysed with multivariate methods [28], commonly partial least squares (PLS), although alternative methods that avoid the need for multivariate analysis have been reported [29]. The range of wavelengths reported varies across the infrared region. Glucose produces absorption bands in the Mid Infrared (MIR) region (from 2.5–10 μm), with peaks around 9.2μm and 9.5μm [30], and has been demonstrated in human subjects [30,31]. The MIR region contains the fundamental vibrational modes and consequently these bands are usually sharp and strong, roughly three orders of magnitude stronger than the higher-order modes observed in the Near Infrared [32]. There has been increasing research into glucose sensing using Quantum Cascade Lasers (QCLs) [33] in MIR region, which offer a high power density and can be tuneable across a range of wavelengths [34,35]. The MIR region is, however, heavily attenuated in tissue, with a limited penetration depth of roughly 10μm [36], although there is increasing interest in photoacoustic spectroscopy using MIR lasers, where studies have reported stronger penetration and shown positive results *in vivo* [37,38]. Together with the low performance of emitters and photodetectors, the MIR region is difficult to use for non-invasive sensing.

Near Infrared (NIR) radiation, from 0.7–2.5 μm, has the advantage of the deepest penetration in tissue, up to several millimetres in the so-called 'biological window' from 900-1600nm [39], and well-developed light source and detector technology. Glucose has absorption peaks in the NIR at 2120 nm, 2270 nm and 2320 nm, caused by C-H bond stretching and the combination band of O-H and CH bond bending [40,41], as well as a second-level excitation (overtone) of the -CH group bond around 1688nm [42]. Higher-order overtones exist at shorter wavelengths but are much weaker in intensity, due to the lower statistical probability of higher excitations, and are hard to distinguish from the spectra of other analytes such as lipids and water. The strong interference from the absorption of lipids and water presents a challenge for the development of commercial glucose sensing devices in the NIR region. The strongest NIR absorption band from water in the NIR biological window is the O-H bond stretch at 1400-1450nm [43], however water absorption is then at a local minimum in the region of the -CH overtone in glucose around 1688nm, which means that this band offers promising potential for glucose quantification. NIR glucose sensing studies have been reported on glucose solutions [44–46], tissue phantoms [47,48] and human subjects [49,50]. Several different NIR optical variations have been reported, including photoplethysmography [51] and the use of lasers as light sources [52,53]; and the choice of optical components for infrared spectroscopy experiments is important.

The aims of this study are threefold. Firstly, by evaluating the performance of different NIR detector systems and light sources, to develop and optimise a NIR spectroscopy system for analysis of liquid-based glucose samples, as part of the initial work towards the development of a NIR sensing device focused on the 1688nm second-level excitation in glucose. Secondly, to use glucose concentration

prediction experiments to determine the limit of detection in aqueous solutions for the optimised system. Thirdly, to test the ability to measure glucose concentration from transmitted and normally scattered light in a simple intralipid phantom. We aim to demonstrate that the system can measure physiological glucose concentrations in solution to a level of accuracy greater than previously reported for dispersive spectrometers in the NIR overtone region.

2. Methods

2.1. Detection System

Three detection systems (A, B & C) were considered for the system, all of which were designed to collect accurate spectra in the NIR region. System A used a miniature infrared spectrometer (Ocean Insight FlameNIR, Ocean Insight, Orlando, US) containing a grating with an array of photodiodes. The system was fully fibre-coupled, with light provided by a broadband halogen light source (Ocean Insight HL2000, Ocean Insight, Orlando, US) of fixed power. The sample was held in a fully enclosed sample holder unit (Ocean Insight SquareOne, Ocean Insight, Orlando, US) which was coupled to the light source and FlameNIR unit by fibre optics (figure 1a). The sample box entrance and exit ports were fitted with identical 5mm Quartz collimating lenses. Light entering the FlameNIR unit was diffracted by the grating and incident on a photodiode array, allowing the optical intensity across each diode to be measured automatically and the resulting spectra constructed. Across the 950-1700nm spectral range, the signal-to-noise ratio (SNR) varied between 10.2dB and 13.6dB. The spectra were automatically collected using the provided OceanView software and the system had a spectral resolution of 5.8nm. Due to the low saturation point of the diode array, a 25% neutral-density filter (ThorLabs NENIR506B, ThorLabs, Newton, US) was placed directly after the sample to reduce the optical intensity whilst the integration time was 5ms, the longest time achievable without the causing the diode to saturate.

System B was a single-photodiode system, using a Czerny-Turner grating monochromator (figure 1b). Near Infrared light was provided by either a halogen lamp or a globar, with the halogen lamp used in the detector experiments to compare with the other two systems. The monochromator (Horiba iHR320, Horiba Jobin-Yvon, France) contained a 600g/cm diffraction grating, which acted as a dispersive element, and an exit mirror which could be automatically controlled to allow single wavelengths to leave the exit port to a precision level of ±0.20nm. Outgoing light was collimated using a 1” CaF_2 lens at the entrance port of the cuvette holder. The holder was an anodised aluminium cube, which was infrared opaque, with windows on four sides and a central well which could hold a 1cm x1cm cuvette (Thorlabs CVH 100, ThorLabs, Newton, US). An adaptor port (Thorlabs CVH 100-COL, ThorLabs, Newton, US) was mounted in the window opposite the entrance port, which contained an in-built CaF_2 lens which focused light on the exit of the adaptor, 20mm away. A Thorlabs SM05PD5A InGaAs photodiode (ThorLabs, Newton, US), operated in photovoltaic mode [54], was positioned at the end of the adaptor to collect the transmitted light. The voltage across the device was measured using a Keithley 2400 (Keithley Instruments, Cleveland, US) Source-Measure Unit (SMU). Across the 700-1800nm range measured, the SNR, which was noise-limited, varied between 16.1dB and 17.6dB. The entire system was located inside an optical box, formed from aluminium panels, which was closed during scans to shield the experiment from background light sources. Data were collected using LabView 2018 (National

Instruments, Austin, US), which simultaneously controlled the SMU and monochromator to record the photodiode voltage at each successive wavelength. The spectral resolution was kept consistently at 5nm and the integration time at 500ms.

System C was a miniaturised Fourier Transform Infrared (FTIR) [55] spectrometer (Ocean Insight NanoQuest, Ocean Insight, Orlando, US) that had the same fibre-coupled arrangement as the FlameNIR in System A, with the HL2000 light and fibre-coupled sample box (figure 1c). The NanoQuest module contained a microelectromechanical (MEMS) interferometer, with one mirror controlled by a MEMS actuator. A photodetector (operating between 1300-2600nm) collected the resulting interferogram, which was then transformed using the Fourier transform to produce the final spectra, with a spectral resolution of between 1.9nm and 3.6nm. The SNR ranged between 31.7dB and 23.6dB. Data were collected using the accompanying NanoQuest software.

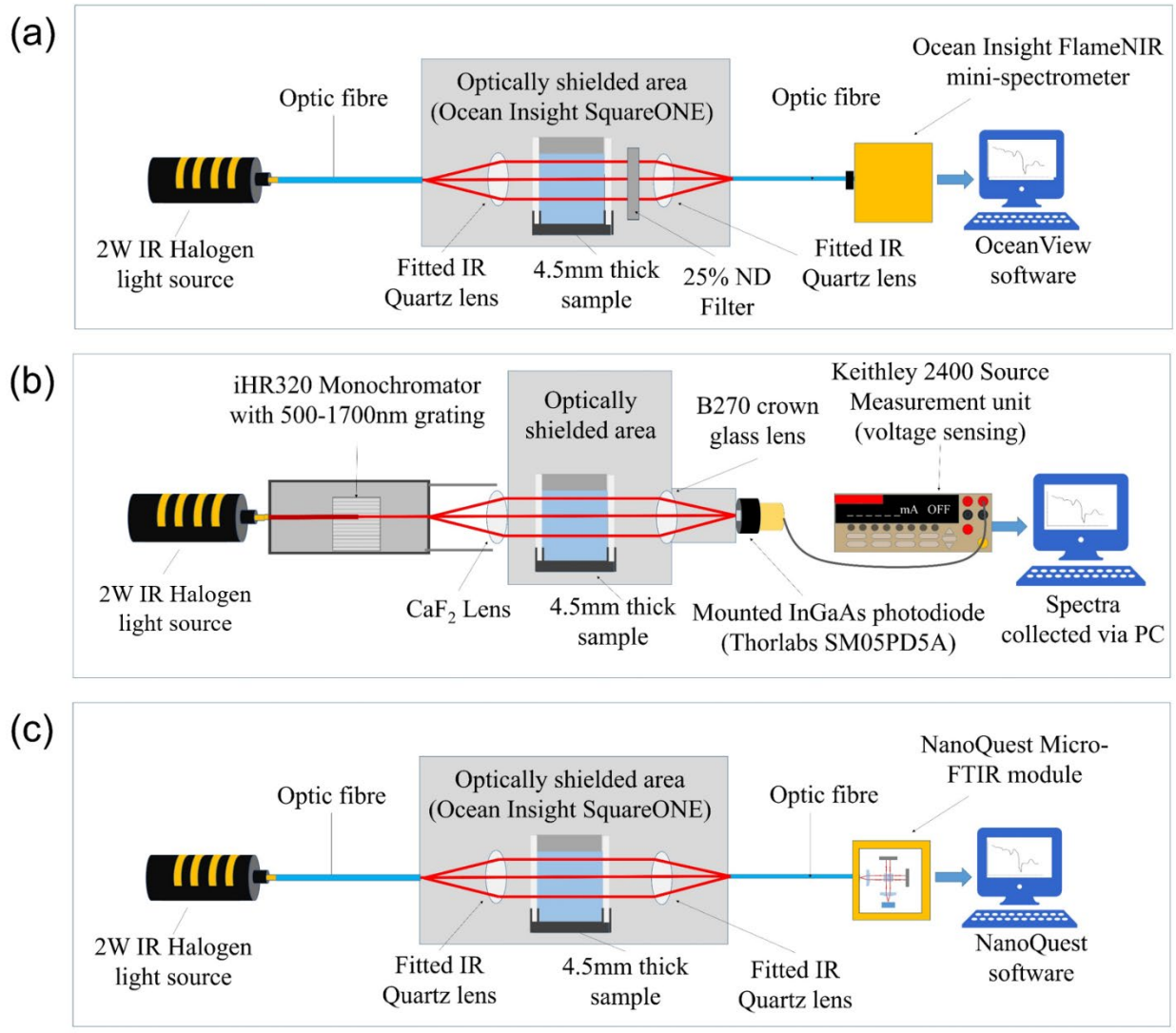

Figure 1: Schematic diagram of the spectroscopy systems. a) FlameNIR miniature spectrometer containing diode array; b) Czerny-Turner monochromator with single InGaAs photodiode; C) NanoQuest miniature FTIR module.

2.2. Light sources

Two different light sources could be fitted to the iHR320 monochromator and the performance of each source was evaluated for the same set of samples. One source was a globar (Horiba LSH-GB, Horiba Scientific, Kyoto, Japan) which consisted of a Silicon Carbide rod heated electrically using a DC power supply (GW-Instek SPS-1230). The globar produced an average broadband optical power of 1mW at the focal point and was coupled such that the focus coincided with the entrance port of the monochromator. The second source, which used the second monochromator entrance slit, was a halogen lamp (Ocean Insight HL2000) which had a fixed output power of 2W. Both light sources were given 30 minutes to warm up prior to each experiment. Before each set of experiments, a background spectrum of the light source was taken and compared to a record of previous spectra to ensure that the intensity was consistent.

2.3. Sample cuvettes

Samples were scanned in 3mL polystyrene cuvettes (Ocean Insight CVD Series, Ocean Insight, Orlando, US) which featured a 4.5 ± 0.2mm thick sample region, which was the shortest achievable path length with this equipment. In preparatory work for this study, several cuvette materials and geometries were tested, including fused IR Quartz, polystyrene and CaF_2. The polystyrene cuvettes showed spectral features in the 700-1800nm region of interest, however these could easily be removed when the spectra were corrected for background. They were chosen because they offered a shorter path length than the quartz alternatives and were also durable, sealable and large enough in size that the full beam from the globar would pass through the sample area.

2.4. Sample preparation

Glucose stocks of 1-100mmol/L were prepared by serial dilution from a 100mmol/L stock, formed by dissolving a fixed mass of D-glucose powder (Sigma-Aldrich G8270 >99.5% D-glucose, Sigma Aldrich, Missouri, US) in de-ionised water. This allowed for a range of concentration steps – from 1mmol/L to 10mmol/L – depending on the design of each part of the study, with a 10mmol/L step used for the optimisation experiments. To model a strongly-scattering scenario, samples were prepared of 10% Intralipid emulsion, since Intralipid can be used to model the scattering properties of numerous tissue layers including the dermis, epidermis and hypodermis [66]. For the intralipid experiments, a 1.4mL volume of each solution was then added to a 1.4mL volume of 20% intralipid emulsion (Sigma-Aldrich I141, Sigma Aldrich, Missouri, US). Negating any change in the solution volume due to the addition of glucose, this process diluted the intralipid emulsion by half, leading to a 10% emulsion. The samples were allowed to stand for half an hour to allow the intralipid temperature to stabilise, and were mixed again before measurement.

2.5. Data Processing & Statistics

Initially, spectra were taken of a 100mmol/L glucose solution, and the SNR of each system compared at 1650nm, an expected glucose absorption band, and 1400nm, where absorption by water is dominant. During each experiment, each sample was scanned five times. For System C the spectra were automatically smoothed and background-corrected by the NanoQuest software. For systems A and B, post-collection analysis and processing of the data was done in two stages. Firstly, the

average raw absorbance was evaluated at 1650nm, a wavelength located within the broad first overtone absorption band of glucose. Absorbance, $A(\lambda)$, was calculated using the Beer-Lambert Law, equation 1, where $I_0(\lambda)$, $I(\lambda)$ are the intensities measured before the sample and after the sample respectively.

$$A(\lambda) = log\left(\frac{I_0(\lambda)}{I(\lambda)}\right) \quad (1)$$

Absorbance was plotted against glucose concentration, a linear fit applied, and the coefficient of determination (R^2) used to judge the strength of the relationship. Although the peak of the band is closer to 1688nm, this was deemed too close to the cut-off wavelength of the System A and System B detectors at 1700nm. All data was checked to ensure that it conformed to the assumptions required for linear regression; that the variables showed a linear relationship and that the residuals were normally distributed, independent and had constant variance. Secondly, to correct for background variation, all spectra were smoothed using a 2nd order Savitzky-Golay filter with 20 points of window, a form of mathematical smoothing filter which derives 2nd order polynomials for each data point based upon a given number of surrounding data points. This polynomial is used to re-calculate that data point and the process is repeated for all points. The second derivative, $d_\lambda^2 I(\lambda)$, was taken for each spectrum – the second derivative is commonly used in spectral processing to remove baseline shifts from the data [56,57] and has been used previously by similar studies [58]. Partial Least Squares (PLS) multivariate regression [59] was then applied to the derivative spectra, using the closest achievable range to 700-1800nm (950-1700nm for System A, 700-1800nm for System B and 1300-1800nm for System C) in 5.8nm steps for System A (128 spectral elements), 5nm steps for System B (221 spectral elements) and 2-3nm steps for System C (199 spectral elements). Leave-one-out cross-validation was performed for each model, and the root mean predicted residual sum of squares used to identify the optimal number of PLS factors for each model. The step size for System C was automatically controlled by the software and unfortunately could not be held constant. Four repeat scans (the training data set) were used to train the model and then the model was used to predict the concentration of a further, independent, scan of the same sample. The standard error of prediction (SEP) was used to evaluate the accuracy of the model. All analysis was carried out in OriginLab 2020b (OriginLab Corp., Northampton, US).

3. Results & Discussion

3.1. System optimisation and development

3.1.1. Detection system

The SNR of the three detection systems varied with wavelength across the 700-1800nm spectral range, with a standard deviation of 1.1dB for system A, 1.2dB for system B and 8.5dB for system C. At 1400nm and 1650nm the SNR values for the three systems were notably different. System A showed the lowest SNR, 10.0dB at 1400nm and 8.1dB at 1650nm. The SNR for system B was 14.7dB at 1400nm and 14.9dB at 1650nm. The SNR for system C was 7.8dB at 1400nm and 20.3dB at 1650nm and was observed to vary, reaching 0dB at both 1470nm and around 1800nm, and 31.6dB around 1300nm. The low SNR indicates that system A was most likely to be affected by strong noise, however the strong changes in SNR between different wavelengths for system C are also notable. The fact that the SNR for this system varied by so much between wavelengths, despite

no strong absorption being expected, suggests the spectra are low quality and the signal unstable. Absorption spectra were collected for aqueous glucose solutions with a 10mmol/L concentration step with each of the detection systems. Figures 2a-c show the averaged absorbance at 1650nm against glucose concentration for systems A, B and C. System A (the FlameNIR system) shows no clear trend against glucose concentration, $R^2 = 0.02$ ($p = 0.68$), with the points heavily scattered, although the variation between successive scans is very small as evidenced by the small error bars. It is likely that the change in absorbance due to slight variation in the cuvette position between samples has a far greater effect than the difference in absorbance due to the samples themselves. There was no also significant relationship between glucose concentration and absorbance for System B, $R^2 = 0.10$ ($p = 0.33$), and only a weak relationship for System C, $R^2 = 0.52$ ($p = 0.01$). For both systems, the error bars heavily overlap, suggesting that the scan intensity may be affected by background noise variations and that smoothing and background correction could improve the data quality. From the raw transmittance data, the sensitivity (change in signal per mmol/L of glucose) of the systems at 1650nm were be calculated. For System B, (excluding 60mmol/L because it is an outlier), the sensitivity was 5.02µV per mmol/L ($R^2 = 0.65$, $p<0.05$), and for System C 1.25 counts per mmol/L ($R^2 = 0.65$, $p<0.05$). System A did not produce a statistically significant trend. The second derivative, with 2nd order Savitzky-Golay filtering, was applied to both datasets, then Partial Least Squares (PLS) regression in OriginLab 2020b was applied to the processed data from systems A, B and C. The number of PLS factors was 1, 6 and 5 for each system respectively. The spectra produced by System C were noisy above 1.8µm and consequently this region was excluded from the modelling. The derivative spectra taken from System C were also too noisy for PLS to be possible, and therefore the processed System C spectra were only smoothed with the SG filter.

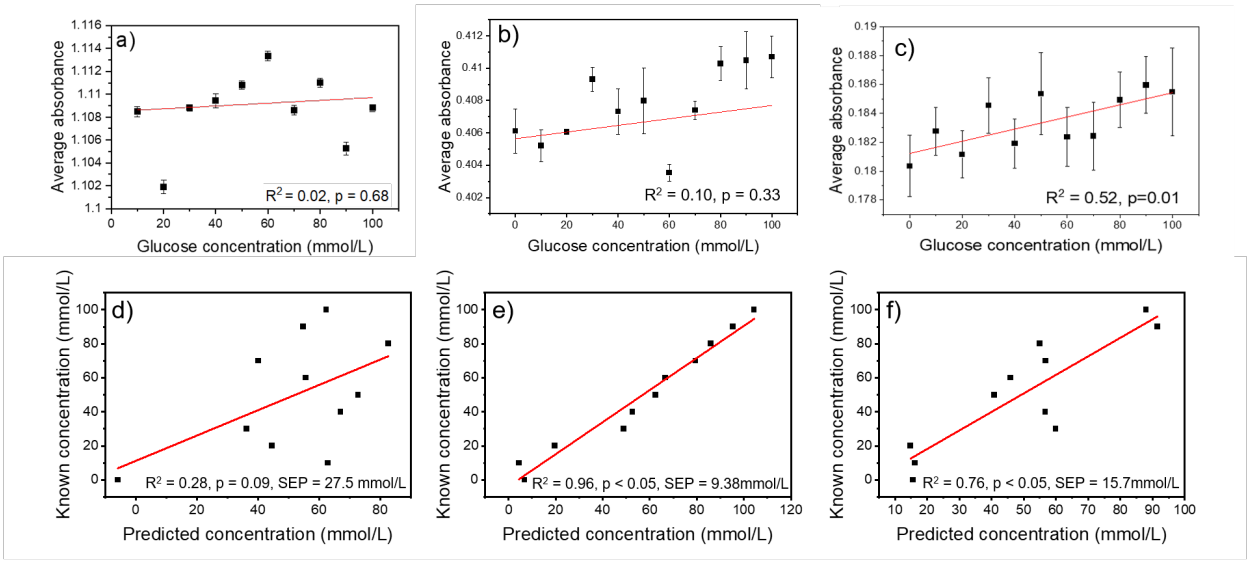

Figure 2: Average absorbance at 1650nm against glucose concentration for (a) System A - the FlameNIR photodiode array, (b) System B - the InGaAs photodiode with grating monochromator and (c) System C - the miniature FTIR module (for which processing was automatically applied to the spectra by the NanoQuest software). Post-processing comparison of predicted and true concentrations for (d) System A - the FlameNIR photodiode array, (e) System B - the InGaAs photodiode with grating monochromator & (f) System C - the miniature FTIR module.

System B produces a stronger relationship, ($R^2 = 0.96$, $p < 0.05$) compared to System A, ($R^2 = 0.28$, $p = 0.09$) and System C ($R^2 = 0.76$, $p < 0.05$). The standard error of prediction is 9.38mmol/L – over half that for System A (27.5mmol/L) and lower than C (15.7mmol/L) (figure 2d-f). There are several possible reasons for the poor performance of System A. Firstly, in order to avoid saturation, the FlameNIR module had to be operated with a very short 5ms integration time since the diodes were shown to saturate with longer integration times (>7ms). The integration time is likely to be too short to collect sufficient photons for an accurate measurement, meaning the output is heavily dominated by optical noise. Since the integration time must be fixed so low, System A would perform better with a lower light intensity, where the diodes would not saturate at longer integration times (such as 500ms used with system B). Observations were made when System A was coupled to the globar light source, which was done by mounting the end of the fibre optic at the focal point of a system of two collimating lenses positioned at a spare monochromator exit slit. With the globar, which had less than 1% of the optical power of the HL2000, the spectrum of the source was accurately obtained in agreement with the spectra produced by System B using the same globar source. However, the optical connection between the monochromator and the FlameNIR would need to be improved, since the spectra of any samples tested were noisy and the two devices could not be made compatible. With System C, the ranges covered by each concentration overlap to a much greater extent than with System B. Given the same light source (halogen lamp) was used with each system, it is not likely that the input optical power limited the reliability of the measurements. However, unlike the FlameNIR in System A, which had a standard InGaAs detector array, the NanoQuest contained a single wavelength-extended InGaAs photodiode with increased Indium content for operation for longer wavelength (1400-2500 nm), however, the degradation of InGaAs leads to a lower spectral responsivity in comparison with the standard InGaAs detector. The SNR of System C was low and is this likely due to this lower responsivity. Additionally, the active area of the wavelength-extended detector is likely to be smaller in System C due to the miniaturised nature of these devices, which further reduces the SNR. Further investigation is required to confirm this and improve this setup. Both systems A and C could be affected by losses in the optical fibre. As described, optical fibres of length 50cm were used to couple the light source to the sample holder and the sample holder to the detector module (approximately 1.5m of fibre in total). There are several sources of fibre loss, and these include absorption by the fibre, scattering and bending losses [60,61]. Whilst it is difficult to identify the exact cause of fibre loss, it is possible that a combination of these losses could attenuate or disperse the signal reaching the detector. Furthermore, it is worth noting that for systems A and C the entire broadband signal was transmitted through the sample, whilst in System B the dispersive element (the monochromator) was placed before the sample, thereby allowing the individual wavelengths to be passed through the system consecutively.

It is evident that System B produces data with the highest accuracy due to its high spectral resolution. Additionally, since this system consists of multiple components, there is potential to modify it for reflectance applications and other optical configurations, which is not possible with the other two detectors. The main disadvantage of System B was the long measurement time due to moving parts in the monochromator, which lengthened the average scan time to over two minutes,

however the improved accuracy over the other systems meant that System B was therefore chosen as the final NIR spectroscopy system.

3.1.2. Light Sources

Figures 3a-b show the average absorbance at 1650nm for the two different light sources, used in conjunction with System B. There is no significant relationship between concentration and absorbance at 1650nm in the raw halogen lamp data ($R^2 = 0.23$, $p = 0.14$), whilst with the globar dataset a trend in the data is apparent, with an R^2 of 0.74 ($p < 0.05$), although the error bars overlap. In the case of the globar, the difference in transmitted light intensity per 10mmol/L of glucose solution is of a similar order of magnitude to the variation due to random fluctuations in the light source power. Indeed, it was observed that the input electrical power to the globar varied by up to 1.6W during the experiment as the input voltage was automatically adjusted by the power supply in order to retain a stable current supply. The power was supplied to the globar via a connecting screw, and the fluctuations in voltage can be attributed to thermal expansion of the globar leading to a poor electrical connection. Ideally this should be investigated by studying the voltage at which the electrical connection becomes damaged, however, this is impractical as the globar must be closed when the voltage is on for safety reasons. However, there was no correlation between the localised voltage drift and the output optical intensity, suggesting that the voltage fluctuations have a random effect on the fluctuations in optical power. The variations in the measured signal may be due to the sensitivity of the detector, and future work should aim to confirm this by quantifying the sources of noise in the detector. For the halogen lamp from the mains supply, no information could be obtained on any fluctuations in input power. However, the error bars are smaller (approximately half the size) for the halogen lamp, which suggests that the globar output is less stable. Future work should aim to investigate the reasons for this using power metre measurements, however that fact that the globar PLS model is not less accurate than that with the halogen lamp suggests that these power fluctuations are not a limiting factor on the accuracy of the data.

Both the processed datasets produce linear trends with correspondingly high R^2 values of 0.99 ($p < 0.05$) and 0.98 ($p < 0.05$) each. This suggests that both datasets are equally accurate after this pre-processing step, which successfully corrects for the various baseline noise observed in the raw data. 100mmol/L was excluded for both datasets as the second derivative was more than 5 standard deviations from the fit. Furthermore, the PLS model predictions shown in figure 3 show strong agreement between the known and predicted concentrations. The optimal number of PLS factors were 2 and 4 respectively. The Standard Error of Prediction (SEP) is similar for the halogen lamp and globar, 3.18 mmol/L and 3.98 mmol/L respectively. To quantify the variation in the standard error of prediction, five further regression models were generated, each model using a different set of scans for training. The standard error of prediction was calculated for each model and the average SEP across all five models was found to be 3.07 ± 0.62 mmol/L for the halogen lamp and 3.05 ± 0.59 mmol/L for the globar. Since the standard deviations overlap, it cannot be concluded that either dataset is definitively more accurate than the other. The two light sources would be equally acceptable choices to use in the prototype spectroscopy system and they both have practical advantages; the optical power of the globar can be controlled using the power supply whereas the power of the halogen lamp is fixed. Conversely, the halogen lamp has the advantage of emitting visible light, making alignment and calibration of the optical elements significantly simpler. Power

metre measurements would allow the spectra of both sources to be collected using an independent method which could be used both for normalisation and to accurately confirm the spectra of both sources, and this should be considered in a further study.

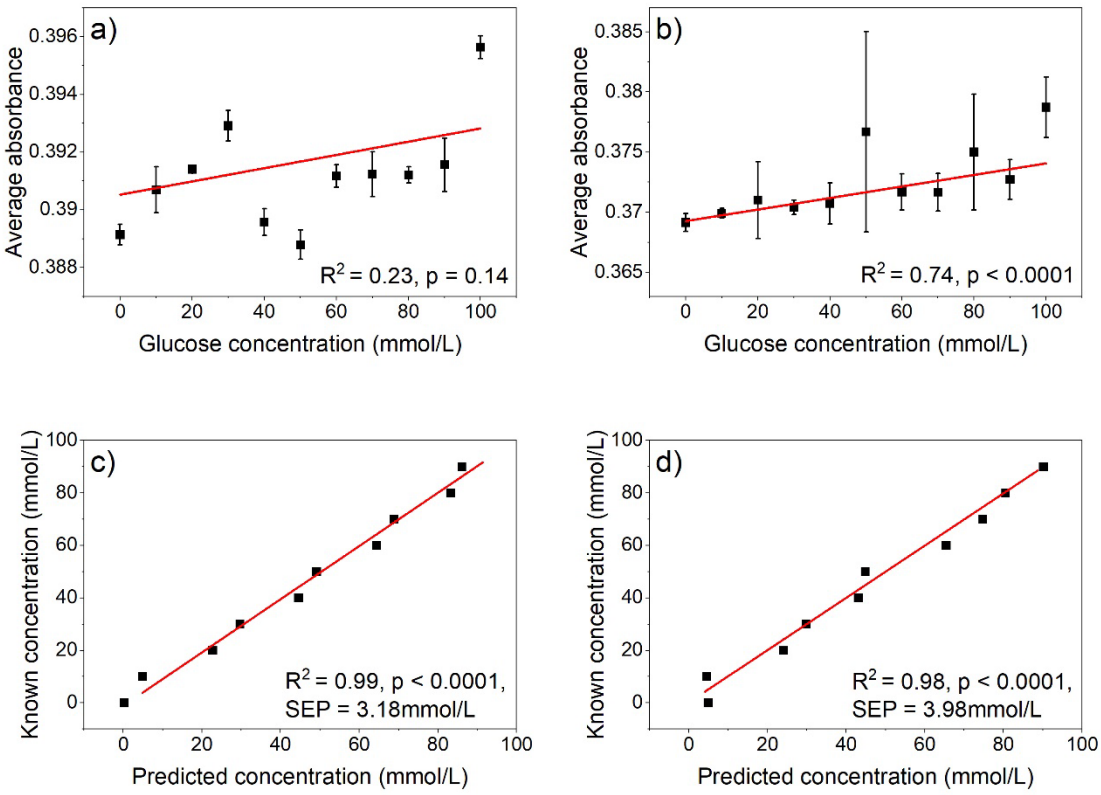

Figure 3: Average absorbance before processing at 1650nm against glucose concentration for (a) Halogen lamp and (b) Globar. Post-processing comparison of predicted and true concentrations for (c) Halogen lamp and (d) Globar.

3.2. Glucose sensing experiments with the optimised system

3.2.1. Aqueous glucose solutions

The optimised prototype spectroscopy setup, using System B (monochromator and InGaAs photodiode) and the globar, was used to study the transmitted light intensity for concentration steps of 10mmol/L, 8mmol/L, 5mmol/L, 4mmol/L, 2mmol/L and 1mmol/L to ascertain the detection limit of the system.

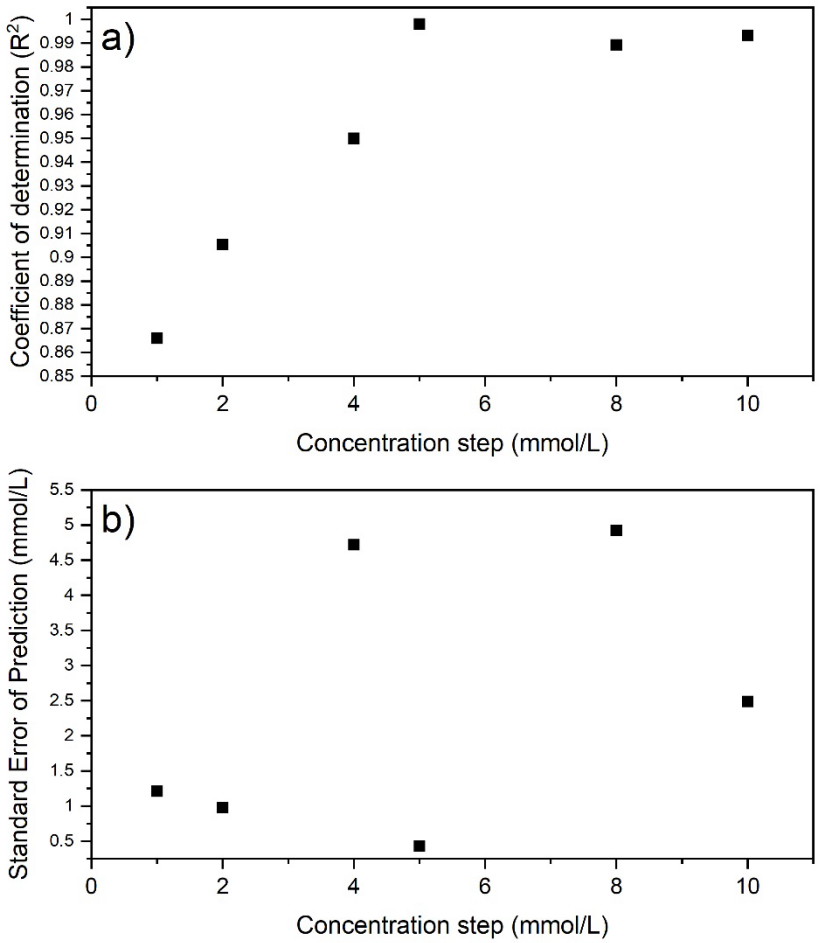

Figure 4: Concentration step against a) Coefficient of determination for the predicted glucose values against concentration step and b) Standard error of prediction against concentration step.

The absorption spectra were smoothed, as previously, with a 2nd order SG filter and PLS regression was applied to the datasets. Figure 4a shows the coefficient of determination (R^2) against concentration step and it can be observed that the R^2 starts to steadily decrease below 5mmol/L, above which it is roughly stable. However, no such trend is present in the SEP values (figure 4b), which appear to vary considerably between concentration steps, suggesting that random error within some of the datasets still has a noticeable effect. For the 1mmol/L and 4mmol/L steps, the uncertainty in concentration is larger than the amount by which the concentration is varied, making accurate prediction challenging. We suggest that 5mmol/L is the current limit of detection, firstly because below this concentration the R^2 begins to fall steadily and secondly since only above this concentration the SEP is smaller than the concentration step itself. It is worth noting that when a larger dataset of 10 repeats was generated the SEP for the 1 mmol/L step reduced to 0.53mmol/L, casting doubt on this conclusion. A greater number of repeated measurements will improve the accuracy of the model, however, the fact that the SEP changes so much, and varies between the different concentration steps, suggests that the intensity is still varying considerably with respect to

the small change which is being detected. Since the entire apparatus was held fixed, and the globar output power did not visibly vary during the experiment, it could also be that inaccuracies in the monochromator mirrors may be causing the data variability. The datasheet listed the wavelength accuracy as ±20nm, however, it was observed that moving the mirrors occasionally caused a noticeable wavelength shift. Whilst these issues were often clear, it raises the possibility that the device may be affected by more subtle initialisation and calibration errors which may affect the intensity of the light being transmitted. It is difficult to definitively test this, since the globar and monochromator cannot be easily decoupled, however, further work is required to confirm the accuracy of the wavelengths being produced by the monochromator. This could be possible by coupling the monochromator exit slit, via fibre, to the FlameNIR module, which has an array of photodiodes and can therefore accurately measure the wavelength of the light being emitted. Furthermore, the InGaAs photodiode was sensitive to changes in temperature as low as 0.1˚C and it is possible that heat from the globar lamp could cause the detection efficiency to vary.

Based on these data, a 5mmol/L step is currently the strongest resolution achievable with this equipment. This level of resolution has not been reported for aqueous glucose solutions in the NIR using a dispersive spectrometry approach, although this resolution is low compared to previous studies, using other wavelength ranges and techniques. Most studies of the spectra of aqueous glucose solutions are in the MIR region, where comparisons are not straightforward due to the much shorter path lengths used. Vrančić et al, using a 9.69μm laser, [44], collected transmission spectra from glucose solutions separated by 1.6mmol/L and identified a noise equivalent concentration of 0.22mmol/L, using a path length of 30μm. Using a 9.66μm laser, Lambrecht et al [62] reported an RMS SEP of 0.83mmol/L; whilst Hasse et al [63] reported an SEP of 0.17mmol/L using a tunable laser in the 8.3-11.1 μm range, also with a path length of 30μm. For solutions of pure glucose, the MIR region is expected to give a more accurate prediction due to the presence of fundamental bands which are strong and sharp. However, as discussed, the poor penetration of MIR radiation in tissue is a challenge to developing an *in vivo* glucose sensing system. In the NIR region, accurate measurement of glucose solutions separated by 0.3mmol/L (5mg/dL) using FTIR, in transmission mode, has been reported by Rondonuwu et al [64], with a standard error of 0.33mmol/L. This study, however, used a shorter path length of 1mm, resulting in reduced overall absorption and therefore more accurate results are to be expected. However, it was reported by Jensen et al [46] that water absorbance causes a reduction in the signal-to-noise ratio in this region of spectra of aqueous glucose (1000-2500nm region) and that a 0.4mm path length optimised the signal-to-noise ratio. By comparison, our system involved a 4.5mm path length, which could likely be too long to obtain detailed spectral information at this wavelength region. A detailed study of the effects of path length on the spatial resolution should be conducted for our system to further investigate this. Strong noise due to water in the 900-1700nm region has also been reported by Yamakoshi et al [65]. Current glucose meters offer a much higher level of accuracy (0.1mmol/L [8,66]) and thus significant improvements to the system resolution will be needed for the final non-invasive sensing device. The Signal-to-noise ratio (SNR) of the spectra, roughly 14dB across the overtone region, is notably low and suggests that it would be difficult to collect glucose spectral information from samples containing more than one analyte.

3.2.2. 10% intralipid suspension

The final part of this study aimed to use the system to measure the glucose concentration in a 10% intralipid suspension, which is an example of a heavily scattering medium. Intralipid has been used as a basic model for the optical properties of the dermis and hypodermis as it has a similar scattering coefficient to collagen and adipose tissue, which are the main scattering centres in these tissues [67,68].

Transmitted and normally scattered light (light scattered by the sample and emitted perpendicular to the direction of propagation) were collected simultaneously. To enable this, a second identical photodiode was mounted on the right-hand side of the cuvette-holder, as illustrated in figure 5, with the window cover removed. Unlike the transmittance detector, the normal scattering detector did not have an adapter with inbuilt lens but instead a small threadable lens directly in front of the detector. The normally reflected light spectra are caused by photons which have been scattered by the sample in a perpendicular direction and aim to give an indication of the potential accuracy of a reflectance-based approach for glucose sensing in highly scattering samples, without requiring the setup to be completely redesigned for a backscattering-based approach.

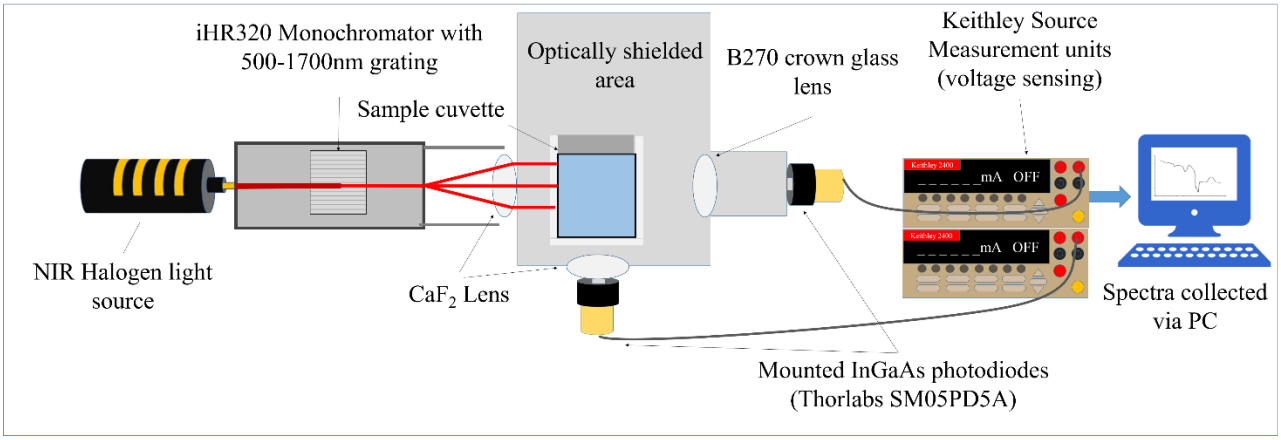

Figure 5: Schematic diagram of the System B spectroscopy system, configured for transmittance and normally reflected light

Scans were taken of aqueous and intralipid based glucose samples with a 5mmol/L sample step, ranging from 0mmol/L to 30mmol/L. Due to the stronger absorption of the intralipid based samples, the halogen lamp, rather than the globar, was used for all experiments in this section due to the much greater optical power it provided. To predict the expected optical power difference between the two detectors, simple Monte-Carlo simulations were run of the cuvette filled with 10% intralipid. The absorption coefficient of 10% intralipid in the NIR range has been previously studied by Thennadil et al [69]. The simulations were run at 1400nm, around the peak of the intralipid spectra, using the MCML Monte-Carlo package developed by Wang et al [70]. The intensity at both detector positions was measured, averaged over five simulations. The number of photons launched was constant for each scan, although it did not correspond to the optical power of the halogen lamp, in order to make an objective comparison between the power received at the two detectors. The transmittance detector was found to receive 10 times the optical power received by the scattering

detector, although experimental observations showed it only received roughly 5 times the power and this is likely due to dispersive losses associated with the different lenses used for the two detectors.

As expected for a long path length, the SNR of the spectral measurements for 10% intralipid at 1650nm was low; taking 7.4dB for the transmitted light and 1.7dB for the scattered light, indicating that the scattered signal is less than an order of magnitude above the background noise. The averaged absorption spectra, calculated from the transmittance data, for the 100mmol/L reference glucose stock solution and 10% intralipid with no glucose added are shown in figure 6a-b, corrected for water and background light. Absorption in the 1600-1700nm overtone band is shown by both samples, with the intralipid showing much stronger absorbance across the spectrum. Thus, in order to initially evaluate the effect of glucose concentration across the spectral range, the transmission data was studied using PLS regression. Figure 6c-d shows the PLS variable importance (VIP), which describes the relative contribution of each wavelength to the model, and the difference between the intralipid samples and the simple aqueous solution is visible. Wavelengths with a VIP less than 0.8 were automatically excluded by the OriginLab PLS algorithm.

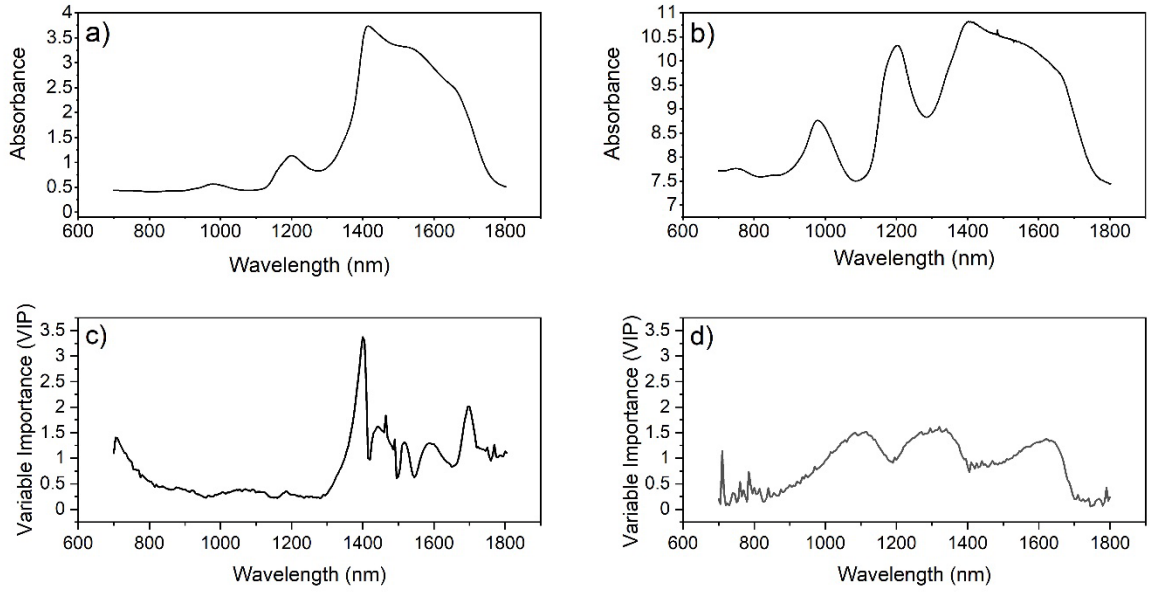

Figure 6: (a) Averaged absorption spectra for a) 100mmol/L glucose stock solution, corrected for water and background light. The glucose solution shows absorption in the 1600-1700nm band, caused by the first CH overtone. Absorption due to OH stretching in water is present around 1400-1450nm. (b) Averaged absorption spectra for 10% intralipid, corrected for water and background light. The magnitude of the absorbance is much stronger and bands are clearly visible at 980, 1200 (2nd order CH stretching overtone) and 1600-1700nm (1st order CH stretching overtone). The steep cut-off beyond 1400nm is due to the detector responsivity. PLS Variable importance plots for (c) aqueous glucose solutions and (d) glucose in 10% intralipid.

In the case of the intralipid, the VIP is broadly constant throughout most of the spectrum, varying between 1 and 1.6 in the 900-1700nm region. Outside this region, the intensity of the signal was low and correspondingly noisy. This suggests that the relationship between glucose concentration

and intensity at each wavelength is roughly constant at most wavelengths. By contrast, in the aqueous solutions the wavelengths around 1400-1600nm have a considerably higher VIP than the rest of the spectrum, with the 1400nm region giving a VIP as strong as 3.6, suggesting that the correlation between glucose concentration and intensity is much stronger at these wavelengths. The 1400-1600nm wavelength region covers the absorption bands of water and glucose and therefore it is likely the case that the absorption bands in the spectrum are mostly being used to generate the PLS model. The fact that this is not the case in the intralipid suggests that the absorption bands are not as dominant in the model and, furthermore, that the transmitted intensity is affected by concentration-dependent scattering throughout the spectrum. Whilst absorption is localised around specific wavelength bands, scattering is roughly constant with wavelength. It is entirely expected that scattering will be present throughout the data, however, the fact that the absorption region does not show a significantly greater VIP suggests that any differences in intensity due to absorption are thoroughly obscured by the change in intensity due to scattering.

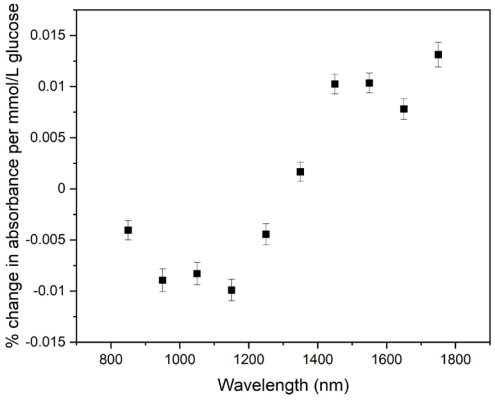

Figure 7: Change in absorbed light per mmol/L of glucose in intralipid in the 850-1750nm range.

The nature of the trend, however, is shown to be more complex in figure 7, which shows the percentage change in absorbed light at wavelengths from 850-1750nm. At wavelengths shorter than 1300nm the trend is positive, which agrees with what would be expected if the samples showed only scattering. Above 1300nm, however, the trend is reversed, suggesting that these data are dominated by absorption. This agrees with previous studies of the optical properties of intralipid through Monte-Carlo modelling and diffuse reflectance spectroscopy. Modelling by Min et al [71] demonstrated that the ratio of scattering coefficient to absorption coefficient increases from around 0 at 1400nm to 50 at 1200nm in 10% intralipid, and this has also been measured experimentally using double-integrating spheres [72]. In the Mie scattering regime, a change in glucose concentration will cause a change in the reduced scattering coefficient. Graaf et al [73] developed an expression for the reduced scattering coefficient due to Mie scattering from dielectric spheres in a medium, where the reduced scattering coefficient (μ_s') varies according to the refractive index mismatch between the spheres and the medium. Larin et al [17] produced a modified form of this result which accounts for the glucose-induced refractive index change (reported as $2.5\text{x}10^{-5}$ mmol^{-1}

by Weast et al [74]), given in equation 2 where ρ is the volume density of the particle, a is the particle radius and m_{medium} is the refractive index of the medium.

$$\mu_s' = 3.28\pi a^2 \rho \left(\frac{2\pi a}{\lambda}\right)^{0.37} \left(\frac{m}{m_{medium}+\delta n_g} - 1\right)^{2.09} \quad (2)$$

As the glucose concentration increases, the refractive index mismatch decreases, causing a corresponding decrease in reduced scattering coefficient. Hence, a greater fraction of the light will be directly transmitted by the sample at higher glucose concentrations, which agrees with the trend observed in the intralipid data below 1350nm. This reduction in scattering has been observed in human tissue [75,76], and in basic phantoms [77]. In the absorption regime above 1300nm, glucose absorption would not be expected to be uniform across such a wide region – this region contains water absorption around 1400nm, glucose around 1600-1700nm and lipids show a clear absorption band at 1720nm due to the first overtone CH stretching mode [78]. However, in the raw spectrum of each sample it was clear that there was a very broad absorption band between 1400nm and 1700nm, which is probably due to the steady increase in absorption at longer wavelengths observed in lipids, water and glucose (with the absorption band appearing to end at 1700nm due to the detector efficiency dropping sharply). Whilst the strong absorption in this region is due to the intralipid, there will also be glucose absorption present, and this will increase at higher glucose concentrations. Without the intralipid, the absorption of water around 1400nm is so strong that it obscures any difference due to glucose concentration.

Figure 8 shows the results of the PLS regression models for the Intralipid for transmittance and reflectance modes with 5mmol/L concentration step. For both datasets, PLS was carried out on both the raw dataset and a processed dataset, where a 2nd order Savitzky-Golay filter and the second derivative were applied to all spectra.

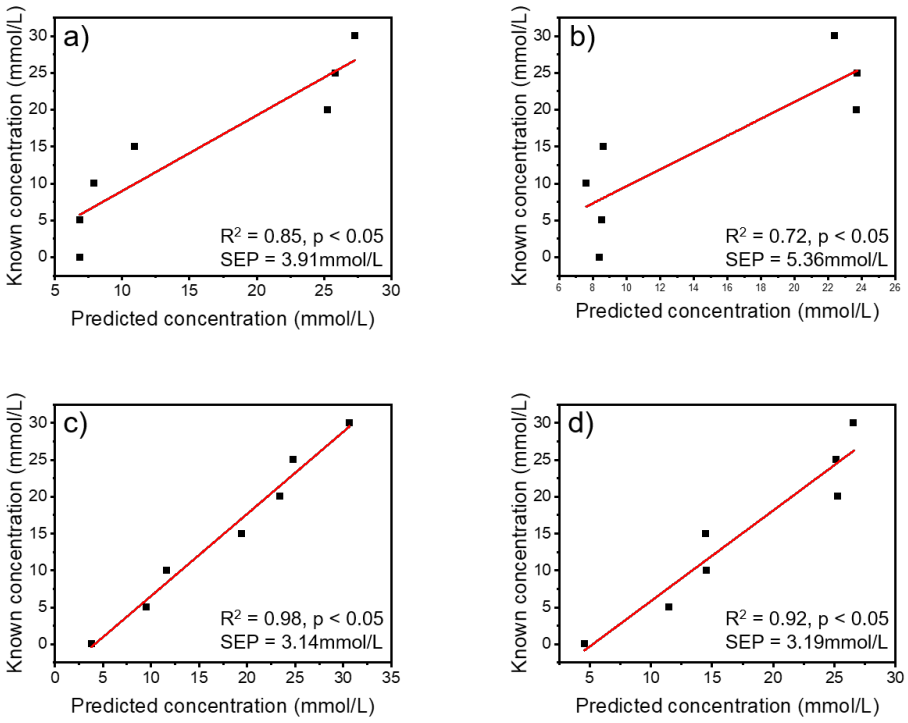

Figure 8: Predicted against known concentration for Intralipid samples with 5mmol/L step. a) Transmittance with no processing, b) transmittance with SG filtering and second derivative, c) a) normal reflectance with no processing, b) normal reflectance with SG filtering and second derivative.

The data in figure 8 shows that the unprocessed reflectance produces the most accurate model (R^2 – 0.98, $p<0.05$), with an SEP of 3.14mmol/L. The second derivative does not improve the model for both transmission and normal reflectance. The second derivative is commonly used as a baseline correction in spectroscopy to correct for any differences present throughout the spectra as a baseline shift. This should work for the aqueous samples, where the spectral curves are expected to be similar outside the regions of strong absorption, however, outside the absorption region the curves are still stratified according to glucose concentration due to scattering. This means that the baseline is not uniform anywhere in the spectrum and therefore a baseline correction will try to remove the effect of scattering and likely damage the ordering in the absorption regions also. More interestingly, the reflectance alignment produces a lower SEP for the intralipid-based samples, despite the scattered detector receiving roughly 10% of the transmitted power. This means that sufficient light is being scattered into a perpendicular direction within the sample to give a measurable difference between different concentrations, which can be used for modelling and prediction. The model is weak, producing an SEP of 3.14mmol/L, however, the transmitted data is similarly weak, with an SEP of 3.91mmol/L. Since the system is to be developed for reflectance measurements, the fact that the normally reflected data produces a more accurate model is promising. Reflectance is a far more versatile configuration than transmittance because it allows spectra to be collected irrespective of

the sample thickness and allows for the optical system to be developed into a moveable detector 'probe' such as the fibre-based devices reported by Maruo et al [29,79] and Uwadaira et al [58].

Finally, a comparison was made between the prediction accuracy of the aqueous and intralipid based samples with 5mmol/L concentration step, in both transmittance and normally reflected mode and with and without processing.

Sample	Raw data SEP (mmol/L)	Processed data SEP (mmol/L)
Aqueous glucose solution transmission	2.94	0.98
Aqueous glucose solution normal reflectance	7.10	9.15
Intralipid transmission	3.91	5.36
Intralipid normal reflectance	3.14	4.19

Table 1: Standard Error of Prediction (SEP) for intralipid-based samples and aqueous glucose samples.

There are three main points from this data. Firstly, the second derivative only improves the accuracy of the model in aqueous glucose transmission. In the case of normally reflected light from the aqueous glucose solutions, there was no discernible trend in the raw data so the second derivative would not be expected to improve the model. The light intensity was, on average, ten times lower than for the transmittance data and contained considerably more noise, which may also be amplified by data processing. There will be no significant scattering centres in an aqueous glucose solution, the size of a water and glucose molecule being vastly smaller than the wavelength of NIR light, and at such low intensity the detector noise, such as thermal effects, become noticeable in the spectra.

Secondly, there is little difference between the unprocessed transmitted and normally reflected data for the intralipid, whereas transmission (2nd derivative) has a markedly lower SEP in the aqueous solutions. This is sensible, since scattering is negligible in aqueous glucose solutions and therefore the fraction of light which is normally reflected will be equally negligible and any data will be heavily dominated by random noise and thus hard to practically use for prediction.

Finally, the aqueous glucose solutions produce the lowest SEP, but only after the second derivative and filter are applied. This suggests that the aqueous samples require baseline correction but after this they show a clear correlation against glucose concentration, whilst the intralipid data are much more scattered. This is likely due to the scattering, which both alters the path lengths of transmitted photons, lengthening them through scattering events, and leads to the glucose dependent scattering change discussed earlier in addition to absorption.

4. Conclusion

In conclusion, this study aimed to develop a Near Infrared spectroscopy system to accurately measure the concentration of glucose in liquid-based samples. The final optimised system consisted

of a Czerny-Turner monochromator and InGaAs photodiode, with light provided by either a globar source or halogen lamp and samples held in 3mL polystyrene cuvettes. The system demonstrated an average SEP of 3.07 ± 0.62 mmol/L with the halogen lamp and 3.05 ± 0.59 mmol/L with the globar, for aqueous glucose solutions with a 10mmol/L concentration step. The optimised system was then used to measure the transmission from aqueous glucose solutions between 1mmol/L and 10mmol/L. A 5mmol/L step was the lowest concentration step at which the SEP was smaller than the step itself, and this level of accuracy has potential to be improved upon using more sophisticated modelling methods and better ways to limit noise and variation in the system. The variation within the data may be caused by monochromator stability issues which require further work to investigate. When spectra were taken for both intralipid and aqueous samples containing the same glucose concentrations with a 2mmol/L step size, the intralipid samples demonstrated optical scattering that varied with glucose concentration in the region below 1300nm, whereas absorption dominated above 1300nm. The SEP was 0.98mmol/L for the aqueous solutions and 2.95mmol/L for the intralipid; the lower level of accuracy resulting from the strong scattering that accompanies absorption with the intralipid samples. The SEP for both transmitted and normally reflected light were similar for the intralipid, suggesting that the scattering is sufficiently strong for reflectance spectroscopy to be possible. This demonstrates potential for the future development of this near infrared spectroscopy system, which will be modified to collect reflected spectra from intralipid-based phantoms using a moveable and freestanding detector configuration. To better approximate an *in vivo* case, further work should also aim to investigate the accuracy of the system for sensing glucose in whole blood. These stages will lead to the development of the data processing needed to accurately predict the glucose concentration and lead to the construction of a prototype in vivo NIR glucose sensing system.

5. Declaration of conflicts of interest

The authors declare that they have no known competing financial interests or personal relationships that could have appeared to influence the work reported in this paper.

6. Funding statement

The authors disclosed receipt of the following financial support for the research, authorship, and/or publication of this article: This work was supported by the Engineering and Physical Sciences Research Council [EP/T518037/1], Joy Welch Educational Charitable Trust and Material Science Lancaster.

7. Data availability statement

Data underlying the results presented in this paper can be obtained from the Lancaster University website, https://www.research.lancs.ac.uk/portal/en/datasets/search.html

8. Ethics statement

Review and/or approval by an ethics committee was not needed for this study because no human participants or animals were involved in this study.

References

1. Davison NB, Gaffney CJ, Kerns JG, Zhuang QD. Recent Progress and Perspectives on Non-Invasive Glucose Sensors. Diabetology . 2022; 3(1):56–71.

2. American Diabetes Association. 2. Classification and Diagnosis of Diabetes. Diabetes Care. 2015;38(Supplement 1):S8–S16.

3. Yates A, Laing I. Diabetes mellitus and hypoglycaemia. In Clinical Biochemistry; Ahmed N, Ed . Oxford, ; New York, : Oxford University Press; 2011.

4. Seuring T, Archangelidi O, Suhrcke M. The Economic Costs of Type 2 Diabetes: A Global Systematic Review. Pharmacoeconomics. 2015;33(8):811–31.

5. Roglic G. WHO Global report on diabetes: A summary. Int J Noncommun Dis. 2016;1(1):3–8.

6. Sun H, Saeedi P, Karuranga S, Pinkepank M, Ogurtsova K, Duncan BB, Stein C, Basit A, Chan JCN, Mbanya JC, Pavkov ME, Ramachandaran A, Wild SH, James S, Herman WH, Zhang P, Bommer C, Kuo S, Boyko EJ, Magliano DJ. IDF Diabetes Atlas: Global, regional and country-level diabetes prevalence estimates for 2021 and projections for 2045. Diabetes Res Clin Pract. 2022 Jan 1;183:109119.

7. Sabu C, Henna TK, Raphey VR, Nivitha KP, Pramod K. Advanced biosensors for glucose and insulin. Biosens Bioelectron. 2019 Sep 15;141:111201.

8. Avari P, Reddy M, Oliver N. Is it possible to constantly and accurately monitor blood sugar levels, in people with Type 1 diabetes, with a discrete device (non-invasive or invasive)? Diabetic medicine. 2020;37(4):532–44.

9. Olczuk D, Priefer R. A history of continuous glucose monitors (CGMs) in self-monitoring of diabetes mellitus. Diabetes & Metabolic Syndrome: Clinical Research & Reviews. 2018 Apr 1;12(2):181–7.

10. Shang T, Zhang JY, Thomas A, Arnold MA, Vetter BN, Heinemann L, Klonoff DC. Products for Monitoring Glucose Levels in the Human Body With Noninvasive Optical, Noninvasive Fluid Sampling, or Minimally Invasive Technologies. J Diabetes Sci Technol . 2021; 16(1):168–214.

11. Tierney MJ, Tamada JA, Potts RO, Jovanovic L, Garg S. Clinical evaluation of the GlucoWatch biographer: a continual, non-invasive glucose monitor for patients with diabetes. Biosens Bioelectron. 2001;16(9):621–9.

12. Kamat DK, Bagul D, Patil PM. Blood Glucose Measurement Using Bioimpedance Technique. Advances in Electronics (Hindawi). 2014;2014.

13. Caduff A, Dewarrat F, Talary M, Stalder G, Heinemann L, Feldman Y. Non-invasive glucose monitoring in patients with diabetes: A novel system based on impedance spectroscopy. Biosens Bioelectron. 2006; 22(5):598–604.

14. Sanai F, Sahid AS, Huvanandana J, Spoa S, Boyle LH, Hribar J, Wang DTY, Kwan B, Colagiuri S, Cox SJ, Telfer TJ. Evaluation of a Continuous Blood Glucose Monitor: A Novel and Non-Invasive Wearable Using Bioimpedance Technology. J Diabetes Sci Technol . 2021; 17(2): 1-9

15. Adeel M, Rahman MM, Caligiuri I, Canzonieri V, Rizzolio F, Daniele S. Recent advances of electrochemical and optical enzyme-free glucose sensors operating at physiological conditions. Biosens Bioelectron. 2020;165: 112331.

16. Yi J, Backman V. Imaging a full set of optical scattering properties of biological tissue by inverse spectroscopic optical coherence tomography. Opt Lett. 2012;37(21):4443–5.

17. Larin K V, Motamedi M, Ashitkov T V, Esenaliev RO. Specificity of noninvasive blood glucose sensing using optical coherence tomography technique: a pilot study. Phys Med Biol. 2003;48(10):1371–90.

18. Larin K V, Eledrisi MS, Motamedi M, Esenaliev RO. Noninvasive Blood Glucose Monitoring With Optical Coherence Tomography A pilot study in human subjects. Diabetes Care. 2002;25(12):2263–7.

19. Zhang Y, Wu G, Wei H, Guo Z, Yang H, He Y, Xie S, Liu Y. Continuous noninvasive monitoring of changes in human skin optical properties during oral intake of different sugars with optical coherence tomography. Biomed Opt Express . 2014; 5(4):990.

20. Lan YT, Kuang YP, Zhou LP, Wu GY, Gu PC, Wei HJ, Chen K. Noninvasive monitoring of blood glucose concentration in diabetic patients with optical coherence tomography. Laser Phys Lett. 2017;14(3):35603.

21. Lundsgaard-Nielsen SM, Pors A, Banke SO, Henriksen JE, Hepp DK, Weber A. Critical-depth Raman spectroscopy enables home-use non-invasive glucose monitoring. Evans CL, editor. PLoS One . 2018; 13(5):e0197134.

22. Pleus S, Schauer S, Jendrike N, Zschornack E, Link M, Hepp KD, Haug C, Freckmann G. Proof of Concept for a New Raman-Based Prototype for Noninvasive Glucose Monitoring. J Diabetes Sci Technol. 2021;15(1):11–8.

23. Purvinis G, Cameron BD, Altrogge DM. Noninvasive Polarimetric-Based Glucose Monitoring: An in Vivo Study. J Diabetes Sci Technol. 2011;5(2):380–7.

24. Sim JY, Ahn CG, Jeong EJ, Kim BK. In vivo Microscopic Photoacoustic Spectroscopy for Non-Invasive Glucose Monitoring Invulnerable to Skin Secretion Products. Scientific Reports 2018 8:1 . 2018; 8(1):1–11.

25. Ghazaryan A, Ovsepian S V, Ntziachristos V. Extended Near-Infrared Optoacoustic Spectrometry for Sensing Physiological Concentrations of Glucose. Front Endocrinol (Lausanne). 2018;9:112.

26. Mayerhöfer TG, Pahlow S, Popp J. The Bouguer-Beer-Lambert Law: Shining Light on the Obscure. Chemphyschem. 2020;21(18):2029–46.

27. Kocsis L, Herman P, Eke A. The modified Beer–Lambert law revisited. Phys Med Biol. 2006;51(5):N91–8.

28. Yadav J, Rani A, Singh V, Murari BM. Prospects and limitations of non-invasive blood glucose monitoring using near-infrared spectroscopy. Biomed Signal Process Control. 2015;18:214–27.

29. Maruo K, Yamada Y. Near-infrared noninvasive blood glucose prediction without using multivariate analyses: Introduction of imaginary spectra due to scattering change in the skin. J Biomed Opt. 2015;20(4):047003.

30. Liakat S, Bors KA, Xu L, Woods CM, Doyle J, Gmachl CF. Noninvasive in vivo glucose sensing on human subjects using mid-infrared light. Biomed Opt Express. 2014 Jul;5(7):2397–404.

31. Kitazaki T, Morimoto Y, Yamashita S, Anabuki D, Tahara S, Nishiyama A, Wada K, Ishimaru I. Glucose emission spectra through mid-infrared passive spectroscopic imaging of the wrist for non-invasive glucose sensing. Scientific Reports 2022 12:1 . 2022; 12(1):1–9.

32. McNichols RJ, Cote GL. Optical glucose sensing in biological fluids: an overview. J Biomed Opt . 2000; 5(1):5–16.

33. Isensee K, Kröger-Lui N, Petrich W. Biomedical applications of mid-infrared quantum cascade lasers-a review. Analyst. 2018; 143(24): 5888–911.

34. Brandstetter M, Genner A, Anic K, Lendl B. Tunable external cavity quantum cascade laser for the simultaneous determination of glucose and lactate in aqueous phase. Analyst . 2010;135(12):3260–5.

35. Chen J, Furukawa H. Rapid and non-invasive detection of high-thickness glucose solution concentrations using quantum cascade laser-based transmission infrared spectroscopy. Infrared Phys Technol. 2023;131:104717.

36. Delbeck S, Heise HM. Evaluation of Opportunities and Limitations of Mid-Infrared Skin Spectroscopy for Noninvasive Blood Glucose Monitoring. J Diabetes Sci Technol. 2021;15(1):19–27.

37. Pleitez MA, Lieblein T, Bauer A, Hertzberg O, von Lilienfeld-Toal H, Mäntele W. In Vivo Noninvasive Monitoring of Glucose Concentration in Human Epidermis by Mid-Infrared Pulsed Photoacoustic Spectroscopy. Anal Chem. 2013;85(2):1013–20.

38. Lubinski T, Plotka B, Janik S, Canini L, Mäntele W. Evaluation of a Novel Noninvasive Blood Glucose Monitor Based on Mid-Infrared Quantum Cascade Laser Technology and Photothermal Detection. J Diabetes Sci Technol . 2020;15(1):6–10.

39. Zhang H, Salo D, Kim DM, Komarov S, Tai YC, Berezin MY. Penetration depth of photons in biological tissues from hyperspectral imaging in shortwave infrared in transmission and reflection geometries. J Biomed Opt. 2016;21(12):126006.

40. Amerov AK, Chen J, Arnold MA. Molar absorptivities of glucose and other biological molecules in aqueous solutions over the first overtone and combination regions of the near-infrared spectrum. Appl Spectrosc . 2004;58(10):1195–204.

41. Beć KB, Grabska J, Huck CW. Near-Infrared Spectroscopy in Bio-Applications. Molecules. 2020;25(12).

42. Golic MI, Alsh KW, Lawson P. Short-Wavelength Near-Infrared Spectra of Sucrose, Glucose, and Fructose with Respect to Sugar Concentration and Temperature. Appl Spectrosc. 2003;57(2).

43. Büning-Pfaue H. Analysis of water in food by near infrared spectroscopy. Food Chemistry. 2003; 82(1): 107–15.

44. Vrancic C, Fomichova A, Gretz N, Herrmann C, Neudecker S, Pucci A, Petrich W. Continuous glucose monitoring by means of mid-infrared transmission laser spectroscopy in vitro. Analyst. 2011;132:1192–8.

45. Chen J, Arnold MA, Small GW. Comparison of combination and first overtone spectral regions for near-infrared calibration models for glucose and other biomolecules in aqueous solutions. Anal Chem . 2004; 76(18):5405–13.

46. Jensen PS, Bak JMY. Near-Infrared Transmission Spectroscopy of Aqueous Solutions: Influence of Optical Pathlength on Signal-to-Noise Ratio. Appl Spectrosc. 2002;56(12):1600–6.

47. Jeon KJ, Hwang ID, Hahn S, Yoon G. Comparison between transmittance and reflectance measurements in glucose determination using near infrared spectroscopy. J Biomed Opt. 2006;11(1):014022–7.

48. Xue J, Ye L, Li C, Zhang M, Li P. Rapid and nondestructive measurement of glucose in a skin tissue phantom by near-infrared spectroscopy. Optik (Stuttg). 2018;170:30–6.

49. Han T, Jin Liu, Rong Liu, Chen W, Yao M, Liu X, Ge Q, Zhang Z, Li C, Wang Y, Zhao P, Sun D, Xu K. In Vivo Near-Infrared Noninvasive Glucose Measurement and Detection in Humans. Appl Spectrosc . 2022 ; 76(9):1100–11.

50. Gayathri B, Sruthi K, Menon KAU. Non-invasive blood glucose monitoring using near infrared spectroscopy. In: 2017 International Conference on Communication and Signal Processing (ICCSP). 2017: 1139–42.

51. Yamakoshi Y, Matsumura K, Yamakoshi T, Lee J, Rolfe P, Kato Y, Shimizu K, Yamakoshi K ichi. Side-scattered finger-photoplethysmography: experimental investigations toward practical noninvasive measurement of blood glucose. J Biomed Opt . 2017;22(6):067001.

52. Fard ST, Hofmann W, Fard PT, Böhm G, Ortsiefer M, Kwok E, Amann MC, Chrostowski L. Optical absorption glucose measurements using 2.3-μm vertical-cavity semiconductor lasers. IEEE photonics technology letters. 2008;20(11):930–2.

53. Vizbaras A, Šimonytė I, Miasojedovas A, Trinkūnas A, Bučiūnas T, Greibus M, Naujokaitė G, Torcheboeuf N, Droz S, Boiko D, Dambrauskas Ž, Gulbinas A, Vizbaras K. Swept-wavelength lasers based on GaSb gain-chip technology for non-invasive biomedical sensing applications in the 1.7-2.5 μm wavelength range. Biomed Opt Express . 2018; 8(10):4834–49.

54. Damulira E, Yusoff MNS, Omar AF, Taib NHM. A Review: Photonic Devices Used for Dosimetry in Medical Radiation. Sensors (Basel) . 2019 May;19(10).

55. Smith BC. Fundamentals of Fourier transform infrared spectroscopy. Boca Raton: CRC Press; 1996.

56. Savitzky A, E MJ. Smoothing and Differentiation of Data by Simplified Least Squares Procedures. Z Physiol Chem . 1951;40(2):1832.

57. Bosch Ojeda C, Sanchez Rojas F. Recent developments in derivative ultraviolet/visible absorption spectrophotometry. Anal Chim Acta. 2004;518(1–2):1–24.

58. Uwadaira Y, Ikehata A, Momose A, Miura M. Identification of informative bands in the shortwavelength NIR region for non-invasive blood glucose measurement. Biomed Opt Express. 2016;7(7):2729–37.

59. Wold S, Sjöström M, Eriksson L. PLS-regression: a basic tool of chemometrics. Chemometrics and Intelligent Laboratory Systems. 2001;58(2):109–30.

60. Peters K. Polymer optical fiber sensors—a review. Smart Mater Struct. 2011; 20(1):013002.

61. Keiser G, Xiong F, Cui Y, Shum PP. Review of diverse optical fibers used in biomedical research and clinical practice. J Biomed Opt . 2014;19(8):080902.

62. Lambrecht A, Beyer T, Hebestreit K, Mischler R, Petrich W. Continuous Glucose Monitoring by Means of Fiber-Based, Mid-Infrared Laser Spectroscopy. Appl Spectrosc. 2006;60(7):729–36.

63. Haase K, Müller N, Petrich W. Towards a continuous glucose monitoring system using tunable quantum cascade lasers. https://doi.org/101117/122291745 . 2018;10490:13–20.

64. Rondonuwu FS, Setiawan A, Karwur FF. Determination of glucose concentration in aqueous solution using FT NIR spectroscopy. J Phys Conf Ser . 2019 ;1307(1):012019.

65. Yamakoshi K ichi, Yamakoshi Y. Pulse glucometry: a new approach for noninvasive blood glucose measurement using instantaneous differential near-infrared spectrophotometry. Journal of Biomedical Optics . 2006;11(5):054028.

66. Tonyushkina K, Nichols JH. Glucose meters: A review of technical challenges to obtaining accurate results. J Diabetes Sci Technol. 2009;3(4):971–80.

67. Chen AI, Balter ML, Chen MI, Gross D, Alam SK, Yarmush ML. Multilayered tissue mimicking skin and vessel phantoms with tunable mechanical, optical, and acoustic properties. Med Phys . 2016; 43(6):3117–31.

68. Pogue BW, Patterson MS. Review of tissue simulating phantoms for optical spectroscopy, imaging and dosimetry. J Biomed Opt . 2006; 11(4):041102.

69. Troy TL, Thennadil SN. Optical properties of human skin in the near infrared wavelength range of 1000 to 2200 nm. J Biomed Opt. 2001;6(2):167–76.

70. Wang L, Jacques SL, Zheng L. MCML—Monte Carlo modeling of light transport in multi-layered tissues. Comput Methods Programs Biomed . 1995; 47(2):131–46.

71. Min X, Liu R, Fu B, Xu K. A preliminary verification of the floating reference measurement method for non-invasive blood glucose sensing. Opt Laser Technol . 2017;91:7–12.

72. Chen C, Lu JQ, Ding H, Jacobs KM, Du Y, Hu XH. A primary method for determination of optical parameters of turbid samples and application to intralipid between 550 and 1630nm. Opt Express . 2006;14(16):7420–35.

73. Graaff R, Aarnoudse JG, Zijp JR, Sloot PMA, de Mul FFM, Greve J, Koelink MH. Reduced light-scattering properties for mixtures of spherical particles: a simple approximation derived from Mie calculations. Appl Opt. 1992; 31(10):1370–6.

74. Weast R. CRC handbook of chemistry and physics. Vol. 54, CRC handbook of chemistry and physics. Florida; 1974. D230 .

75. Maier JS, Walker SA, Fantini S, Franceschini MA, Gratton E. Possible correlation between blood glucose concentration and the reduced scattering coefficient of tissues in the near infrared. Opt Lett. 1994; 19(24):2062–4.

76. Bruulsema JT, Hayward JE, Farrell TJ, Patterson MS, Heinemann L, Berger M, Koschinsky T, Sandahl-Christiansen J, Orskov H, Essenpreis M, Schmelzeisen-Redeker G, Böcker D. Correlation between blood glucose concentration in diabetics and noninvasively measured tissue optical scattering coefficient. Opt Lett. 1997; 22(3):190–2.

77. Kohl M, Essenpreis M, Cope M. The influence of glucose concentration upon the transport of light in tissue-simulating phantoms. Phys Med Biol. 1995;40(7):1267–87.

78. Cozzolino D, Murray I, Chree A, Scaife JR. Multivariate determination of free fatty acids and moisture in fish oils by partial least-squares regression and near-infrared spectroscopy. LWT - Food Science and Technology. 2005;38(8):821–8.

79. Maruo K, Tsurugi M, Tamura M, Ozaki Y. In Vivo Noninvasive Measurement of Blood Glucose by Near-Infrared Diffuse-Reflectance Spectroscopy. Appl Spectrosc. 2003;57(10):1236–44.